Optics Letters

Femtosecond laser point-by-point Bragg grating inscription in BDK-doped step-index PMMA optical fibers

Xuehao Hu,[1,2,*] Zhen Chen,[1,2] Xin Cheng,[3] Rui Min,[4] Hang Qu,[1,2] Christophe Caucheteur,[5] and Hwa-Yaw Tam[3]

[1]Research Center for Advanced Optics and Photoelectronics, Department of Physics, College of Science, Shantou University, Shantou, Guangdong 515063, China
[2]Key Laboratory of Intelligent Manufacturing Technology of MOE, Shantou University, Shantou, Guangdong 515063, China
[3]Photonics Research Centre, Department of Electrical Engineering, The Hong Kong Polytechnic University, Kowloon, Hong Kong SAR, China
[4]Center for Cognition and Neuroergonomics, State Key Laboratory of Cognitive Neuroscience and Learning, Beijing Normal University at Zhuhai, Zhuhai, Guangdong 519087, China
[5]Department of Electromagnetism and Telecommunication, University of Mons, Boulevard Dolez 31, 7000 Mons, Belgium
*Corresponding author: xhhu3@stu.edu.cn

Received 1 December 2021; accepted 3 December 2021; posted 3 December 2021; published 5 January 2022

In this paper, the inscription of 2-mm-long fiber Bragg gratings (FBGs) on benzyl dimethyl ketal (BDK)-doped poly(methyl methacrylate) (PMMA) optical fibers by means of a femtosecond laser and a point-by-point FBG inscription technique is reported. The highest reflectivity of approximately 99% is obtained with a pulse energy of 68.5 nJ, showing a large refractive index modulation amplitude of 7.2×10^{-4}. Afterwards, grating stabilities at room and higher temperatures of up to 80°C are investigated.

https://doi.org/10.1364/OL.450047

Since the first fabrication of fiber Bragg gratings (FBGs) in poly(methyl methacrylate) (PMMA) polymer optical fiber (POF) [1], their sensing applications have been developed for over two decades. Compared to silica fibers, POFs have unique properties; for example, a larger thermo-optic coefficient, a smaller Young's modulus, and good biocompatibility. Thus, FBG-based POF sensors have been widely used for different sensing applications, such as temperature, strain, and humidity [2,3]. Meanwhile, FBGs have been successfully inscribed in various polymers, such as the cyclic olefin copolymer TOPAS [4], the cyclic transparent amorphous fluoropolymer CYTOP [5], the cyclic olefin polymer ZEONEX [3,6,7], and polycarbonate (PC) [8].

In terms of performing FBG inscription, a method combining a UV laser and the phase mask technique remains the most popular one to date. In 2002, Liu *et al.* manufactured a highly reflective (reflectivity 99.8%) grating in a PMMA-based POF using a 325 nm laser. However, the exposure time was 85 min, making it very time consuming [9]. In 2019, Min *et al.* used a 266 nm laser to fabricate an FBG in a pure PMMA two-ring microstructured POF (mPOF) with an exposure time of approximately 2 min and a reflectivity of 50% [10]. In 2011, Yuan *et al.* inscribed an FBG by means of a 325 nm laser in a TOPAS mPOF for 338 min to achieve a grating reflectivity of approximately 70% [11]. In 2016, Koerdt *et al.* fabricated FBGs in multimode CYTOP fibers with a 248 nm pulsed laser, and the reflectivity was approximately 70% with a laser irradiation of 42 min [12]. In 2020, Cheng *et al.* produced an FBG with a reflection strength of 20 dB in an all ZEONEX step-index POF with a single 25 ns pulse at 248 nm [7]. In 2016, Fasano *et al.* inscribed FBGs in PC mPOFs using a 325 nm laser with an average photo-writing time of 6 min, and the strength of the reflected peak was 25 dB [8].

Researchers have also been pursuing higher-quality FBGs by designing POFs with photosensitive cores, so that highly reflective FBGs can be obtained in a short inscription time. Among various types of photosensitive materials, benzyl dimethyl ketal (BDK) is the most promising one for promoting FBG inscription in POFs. BDK acts as a photoinitiator and absorbs at two main wavelengths (approximately 250 and 344 nm). Its refractive index increases as a function of UV light irradiation [13]. In 2017, Pospori *et al.* reported the inscription of an FBG with a reflectivity of 98.4% in a BDK-doped PMMA mPOF using only one krypton fluoride laser pulse [14]. In 2018, Pereira *et al.* produced an FBG with a reflectivity of 84% in a BDK-doped PMMA mPOF using a single pulse at 266 nm [15]. In 2021, Hu *et al.* reported an FBG with a reflectivity of 97.1% in a BDK-doped step-index PMMA POF that was achieved using a single 266 nm laser pulse, and concluded that both the formation of the benzyl molecules and the substitution of the PMMA side chains by initiating radicals due to UV irradiation could be the main reasons for the rapid and large refractive index increase of the BDK-doped PMMA material [16].

Though phase mask technology is convenient for the mass production of FBG, direct writing technologies such as point-by-point (PbP) and line-by-line (LbL) present the unique advantages of high accuracy and high quality along with a reduced thermal effect, because refractive indices can be modified at the sub-micron scale inside transparent materials by a focused

femtosecond laser beam utilizing an objective with a high magnification [17]. In 2015, Lacraz *et al.* inscribed a four-order FBG with a reflectivity of 70% in a CYTOP fiber by the LbL technique with 517 nm femtosecond pulses [18]. In 2021, Chah *et al.* also produced four-order FBGs in CYTOP fibers by the LbL technique, but with 800 nm femtosecond pulses [19]. In the same year, Dash *et al.* inscribed four-order FBGs in all-ZEONEX step-index POFs using a 520 nm femtosecond laser and the PbP technique [3]. In 2015, Hu *et al.* demonstrated the first tilted-fiber Bragg-grating-based surface plasmon resonance with a tilt angle of 6° in a step-index PMMA POF for surrounding refractive index measurements in the range of 1.408–1.428 [20]. However, lower refractive index monitoring requires a greater tilt angle [21]. Generally, a direct writing technique with femtosecond pulses does not need photosensitive fibers to inscribe FBGs; however, larger refractive index changes in POFs caused by higher pulse energies could induce higher transmission losses because POFs normally feature lower melting points compared to silica fibers.

Motivated by the demand for large refractive index changes in POFs for the potential fabrication of highly tilted FBGs in POFs by the plane-by-plane direct writing technique for refractometric measurement, as reported previously for silica fiber [22], in this work, highly reflective FBGs are inscribed in photosensitive POFs by the PbP direct writing technique. We report the inscription of four first-order 2-mm-long FBGs with varied pulse energies in BDK-doped PMMA POFs using a 520 nm femtosecond laser. The highest reflectivity reaches up to approximately 99%. After that, the evolutions of the gratings at room and higher temperatures of up to 80°C are investigated. Also, the mechanism of the refractive index change is discussed.

The single-mode fiber was produced at The Hong Kong Polytechnic University by a pull-and-through method [23] and had core and cladding diameters of 5.6 μm and 125 μm, respectively [24]. Before fiber drawing, the preform was fully annealed to increase the fiber performance in a similar way to the method described in Ref. [25]. FBG inscriptions were performed at Shantou University. The femtosecond laser (SpOne-8-SHG, Newport) featured a pulse duration of 306 fs, a maximal repetition rate of 200 kHz, and a maximal pulse energy E of 28.2 μJ. The linearly polarized beam passed through a tunable half-waveplate and a Glan laser polarizer followed by a collimator and a quarter-wave plate to not only control the pulse energy but also transform the beam polarization from linear to circular, thus reducing the anisotropy of the refractive index change induced by the laser pulses [26]. An oil-immersion objective (60×, NA = 1.42, UPLXAPO60XO, Olympus) was used to focus the beam on the fiber core, which was mounted on a multi-axis tilt platform (M-37, Newport) integrated on three-axis precision translation stages (X/Y: XMS100-S, Z: M-VP-5ZA, Newport). The FBG inscription setup is illustrated in Fig. 1. The reflection and transmission spectra from the gratings were monitored by an FBG interrogator (FS22SI, HBM FiberSensing) with a wavelength resolution of 1 pm and a scanning rate of 1 Hz [16].

Prior to grating inscription, a small piece of fiber was spliced to two fiber pigtails by UV curing [27]. For PbP inscription, the grating period Λ is determined by the ratio of the translation velocity to the pulse repetition rate f. In this work, f was kept constant at 50 Hz, while v was varied to achieve FBGs 1–4, which were closely distributed in a single fiber. Both the reflected and transmitted amplitude spectra of the 2-mm-long FBGs are shown in Fig. 2. The reflectivity R ranged from 64.0% to 98.8% and was calculated by

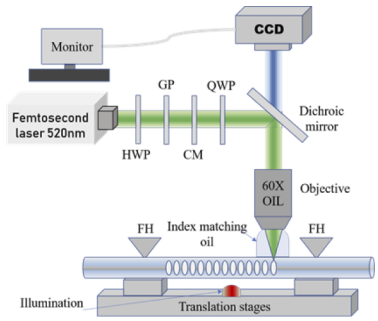

Fig. 1. Illustration of the setup for PbP FBG inscription. HWP: half-wave plate, GP: Glan polarizer, CM: collimator, QWP: quarter-wave plate, FH: fiber holder.

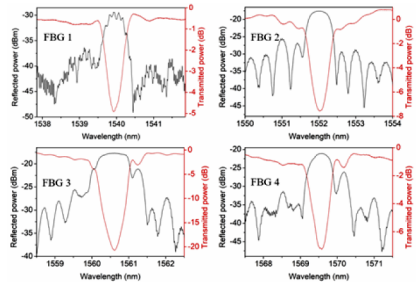

Fig. 2. Reflected and transmitted amplitude spectra for the 2-mm-long FBGs 1–4 just after inscription.

$$R = 1 - 10^{\frac{-A}{10}}, \tag{1}$$

where A represents the transmission rejection amplitude. The photoirradiation-induced out-of-band insertion losses of the four gratings were observed to be between 0 and 1 dB. More grating data are displayed in Table 1.

It was found that the grating reflectivity increased as a function of E, and the highest reflectivity of 98.8% appeared for FBG 3 with 68.5 nJ. It decreased to 75.9% for FBG 4. In order to understand the mechanism of the refractive index change, the grating-induced effective indices n_{eff} and index modulation amplitudes Δn_{eff} were explored. The n_{eff} of the grating is calculated by [28]

$$\lambda_B = 2n_{eff}\Lambda, \tag{2}$$

where λ_B represents the central wavelength of the Bragg mode. Δn_{eff} can be obtained by

$$R = \tanh^2\left(\frac{\pi}{\lambda_B}\Delta n_{eff} L\right), \tag{3}$$

where L represents the grating length, which was 2 mm in this work. It is well known that the refractive index of BDK-doped PMMA material increases with UV irradiation [13]. However, compared to FBG 2, the n_{eff} of FBG 3 with higher pulse energy decreased from 1.50976 to 1.50929, while the Δn_{eff} increased from 3.5×10^{-4} to 7.2×10^{-4}. This phenomenon could be attributed to the boost of the movement of the initiating radicals from non-irradiated to irradiated area . Furthermore, for the highest pulse energy, 71.1 nJ, the n_{eff} and Δn_{eff} of FBG 4 were 1.50919 and 3.3×10^{-4}, respectively, which were smaller than their counterparts for FBG 3. This phenomenon could be caused by the evaporation of certain amount of BDK above 100°C [16].

High-resolution microscope images of FBGs 1–4 are displayed in Fig. 3. The modifications of their refractive indices

Table 1. Data for FBGs Inscribed by the Femtosecond Laser at 520 nm

FBG	E (nJ)	v (μm/s)	Λ (μm)	λ_B (nm)	n_{eff}	R (%)	Δn_{eff} ($\times 10^{-4}$)
1	63.5	25.5	0.510	1539.92	1.50973	64.0	2.7
2	66.0	25.7	0.514	1552.03	1.50976	79.2	3.5
3	68.5	25.85	0.517	1560.61	1.50929	98.8	7.2
4	71.1	26	0.520	1569.56	1.50919	75.9	3.3

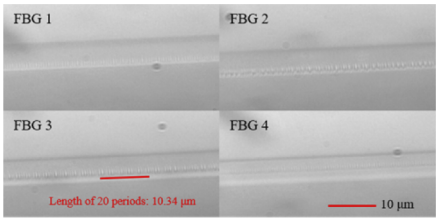

Fig. 3. Optical microscope images of FBGs 1–4 inscribed by the femtosecond laser at 520 nm.

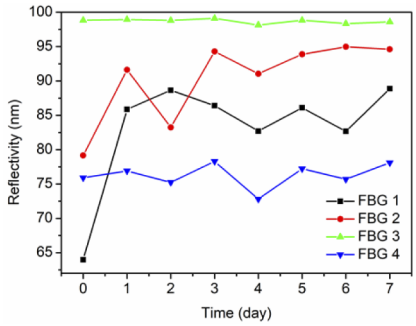

Fig. 4. The reflectivity evolutions of FBGs 1–4 recorded for 7 days after grating inscription at room temperature.

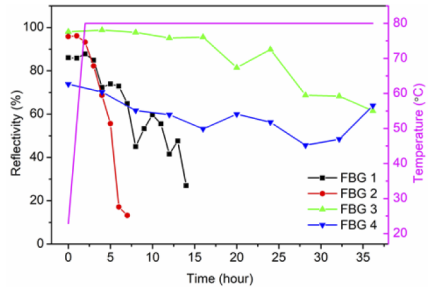

Fig. 5. The reflectivity evolutions of FBGs 1–4 during the annealing process at 80°C for 36 h.

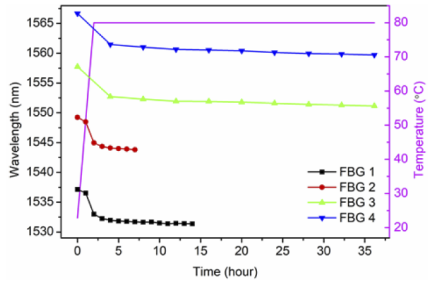

Fig. 6. The wavelength evolutions of FBGs 1–4 during the annealing process at 80°C for 36 h.

induced by the femtosecond laser pulses are clearly visible, although the fringe visibilities for FBGs 1 and 4 are lower than those for FBGs 2 and 3. The index modification size is around 300 nm along the fiber axis. Compared to the size of the beam at the focus, such a small index modification size could be due to a nonlinear effect such as multi-photon absorption [29], as the BDK-doped core has a high absorption peak at approximately 250 nm [13].

Afterwards, the spectra for FBGs 1–4 were recorded for 7 days at room temperature. The evolutions of the grating reflectivities are shown in Fig. 4. Time zero on the horizontal axis represents the moment just after inscription. It was found that for FBGs 1 and 2 with lower pulse energies, the reflectivities increased during the first day. In particular, the reflectivity of FBG 2 increased to 94.6%. This increase in grating reflectivity could be due to the residual initiating radicals generated during photoirradiation, which continued to react after grating inscription. Both gratings were stable for the following 6 days. For FBGs 3 and 4 with higher pulse energies, the reflectivity remained almost the same as that just after inscription, indicating stable properties. It is worth mentioning that the grating evolutions were investigated before the post-annealing process, and the stable grating properties make the potential refractometric measurement feasible based on highly tilted FBGs in POFs at room temperature.

Following that, post-annealing at 80°C was conducted for 36 h in an oven. Figure 5 depicts the reflectivity evolutions of FBGs 1–4 as a function of time. It was found that for FBGs 1 and 2 with lower pulse energies, the reflectivity declined dramatically within 14 and 7 h, respectively, after which the grating peaks in the transmission spectra were difficult to discern (reflectivity ~ 0). For FBGs 3 and 4 with higher pulse energies, the reflectivity decreased to approximately 60% after 36 h, indicating a relatively low rate of decrease. However, to ensure that the grating did not disappear, the annealing process was terminated after 36 h. The reflectivity decreases of FBGs 1–4 can be attributed to the instability of benzyl and the substituted side chains of PMMA, especially for lower pulse energies. Additionally, the wavelength blueshifts of these gratings during the annealing process are shown in Fig. 6; these blueshifts may have been caused by the release of the frozen-in stress generated during the fiber drawing process [30] and the negative thermo-optic coefficient of PMMA [31]. It was found that for FBGs 3 and 4, the wavelength shifts did not stabilize within 36 h.

After post-annealing at 80°C for 36 h, the reflectivities of FBGs 3 and 4 were recorded at room temperature for 6 weeks. They remained at a value of approximately 60%, the same value as observed just after annealing at 80°C. Then FBGs 3 and 4 were heated at 50°C for 36 h, and the results suggested that their reflectivities remained stable, as shown in Fig. 7. The stable reflectivities of FBGs 3 and 4 could have been due to the previous post-annealing at 80°C for 36 h, which would have removed the most unstable benzyl and substituted side chains of PMMA. At the lower temperature of 50°C, Δn_{eff} remained. Figure 8 shows that their Bragg wavelengths varied for the first 16 h

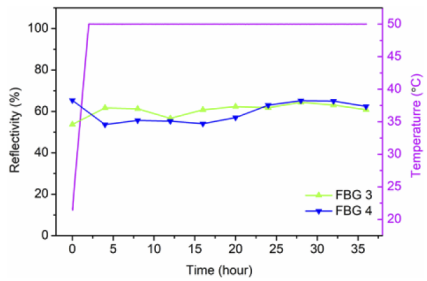

Fig. 7. The reflectivity evolutions of FBGs 3 and 4 at 50°C for 36 h.

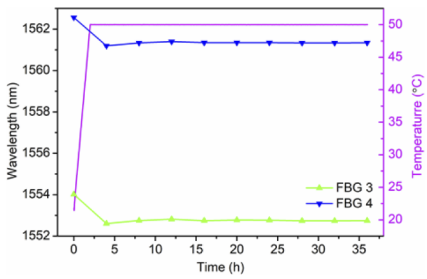

Fig. 8. The wavelength evolutions of FBGs 3 and 4 at 50°C for 36 h.

and then remained stable, in contrast to the previous annealing process at 80°C, during which the properties were not stable. This phenomenon could be caused by the previous release of the frozen-in stress at 80°C and an inability to release the frozen-in stress at the lower temperature of 50°C, which is far from the glass transition temperature T_g (105°C) of the fiber material, PMMA [32]. The stable reflectivity and Bragg wavelength at 50°C ensure that the POF-based FBGs are suitable for biomedical applications, as the human body temperature is normally below 45°C [23].

In this Letter, we first investigated first-order FBG inscription in BDK-doped step-index PMMA POFs, for which the highest reflectivity was 98.8%. The large refractive index change paves the way to the fabrication of highly tilted FBGs in POFs. Afterwards, the FBG spectral evolutions were recorded as a function of time, and good stabilities at room temperature were observed. The performances obtained were related to the pulse energies and can be explained by the existence of residual initiating radicals produced under femtosecond laser irradiation and their subsequent reactions. After that, the FBGs were annealed at 80°C for 36 h, but with decay during the annealing. Later, at 50°C, the gratings presented high stabilities, making them suitable for biomedical applications.

Funding. 2020 Li Ka Shing Foundation Cross-Disciplinary Research Grant (2020LKSFG01B, 2020LKSFG14B); Specialized Project Fund in Science and Technology of Guangdong Province (2019ST096, 2019ST135); Special projects in key fields of colleges and universities in Guangdong Province (2020ZDZX3035, 2020ZDZX3037); The Start-up fund from Shantou University (NTF18016, NTF19023); National Natural Science Foundation of China (62003046); International Science and Technology Cooperation Programme (BZ2019063, BZ2020030, BZ2020045).

Acknowledgment. C. Caucheteur is supported by the F.R.S.-FNRS.

Disclosures. The authors declare no conflicts of interest.

Data availability. Data underlying the results presented in this paper are not publicly available at this time but may be obtained from the authors upon reasonable request.

REFERENCES

1. Z. Xiong, G. D. Peng, B. Wu, and P. L. Chu, IEEE Photonics Technol. Lett. **11**, 352 (1999).
2. C. Broadway, R. Min, A. G. Leal-Junior, C. Marques, and C. Caucheteur, J. Lightwave Technol. **37**, 2605 (2019).
3. J. N. Dash, X. Cheng, D. S. Gunawardena, and H.-Y. Tam, Photonics Res. **9**, 1931 (2021).
4. I. P. Johnson, W. Yuan, A. Stefani, K. Nielsen, H. K. Rasmussen, L. Khan, D. J. Webb, K. Kalli, and O. Bang, Electron. Lett. **47**, 271 (2011).
5. A. Theodosiou and K. Kalli, Opt. Fiber Technol. **54**, 102079 (2020).
6. G. Woyessa, H. K. Rasmussen, and O. Bang, Opt. Fiber Technol. **57**, 102231 (2020).
7. X. Cheng, D. S. Gunawardena, C.-F. J. Pun, J. Bonefacino, and H.-Y. Tam, Opt. Express **28**, 33573 (2020).
8. G. Woyessa, A. Fasano, C. Markos, H. K. Rasmussen, and O. Bang, IEEE Photonics Technol. Lett. **29**, 575 (2017).
9. H. Y. Liu, G. D. Peng, and P. L. Chu, IEEE Photonics Technol. Lett. **14**, 935 (2002).
10. R. Min, L. Pereira, T. Paixão, G. Woyessa, P. André, O. Bang, P. Antunes, J. Pinto, Z. Li, B. Ortega, and C. Marques, Opt. Express **27**, 38039 (2019).
11. W. Yuan, D. J. Webb, K. Kalli, K. Nielsen, A. Stefani, H. K. Rasmussen, and O. Bang, Proc. SPIE **7753**, 77538X (2011).
12. M. Koerdt, S. Kibben, O. Bendig, S. Chandrashekhar, J. Hesselbach, C. Brauner, A. S. Herrmann, F. Vollertsen, and L. Kroll, Mechatronics **34**, 137 (2016).
13. Y. Luo, O. Zhang, H. Liu, and G. D. Peng, Opt. Lett. **35**, 751 (2010).
14. A. Pospori, C. A. F. Marques, O. Bang, D. J. Webb, and P. André, Opt. Express **25**, 9028 (2017).
15. L. Pereira, R. Min, X. Hu, C. Caucheteur, O. Bang, B. Ortega, C. Marques, P. Antunes, and J. L. Pinto, Opt. Express **26**, 18096 (2018).
16. X. Hu, X. Yue, X. Cheng, S. Gao, R. Min, H. Wang, H. Qu, and H.-Y. Tam, Opt. Lett. **46**, 2864 (2021).
17. M. Beresna, M. Gecevilus, and P. G. Kazansky, Adv. Opt. Photonics **6**, 293 (2014).
18. A. Lacraz, M. Polis, A. Theodosiou, C. Koutsides, and K. Kalli, IEEE Photonics Technol. Lett. **27**, 693 (2015).
19. K. Chah, I. Chapalo, Y. Nan, D. Kinet, P. Mégret, and C. Caucheteur, Opt. Lett. **46**, 4272 (2021).
20. X. Hu, P. Mégret, and C. Caucheteur, Opt. Lett. **40**, 3998 (2015).
21. J. Albert, L.-Y. Shao, and C. Caucheteur, Laser Photonics Rev. **7**, 83 (2013).
22. A. Ioannou, A. Theodosiou, K. Kalli, and C. Caucheteur, Opt. Lett. **43**, 2169 (2018).
23. J. Bonefacino, H.-Y. Tam, T. S. Glen, X. Cheng, C.-F. J. Pun, J. Wang, P.-H. Lee, M.-L. V. Tse, and S. T. Boles, Light: Sci. Appl. **7**, 17161 (2018).
24. X. Cheng, Y. Liu, and C. Yu, Micromachines **10**, 717 (2019).
25. C. A. F. Marques, A. Pospori, G. Demirci, O. Çetinkaya, B. Gawdzik, P. Antunes, O. Bang, P. Mergo, P. André, and D. J. Webb, Sensors **17**, 891 (2017).
26. G. Cheng, K. Mishchik, C. Mauclair, E. Audouard, and R. Stoian, Opt. Express **17**, 9515 (2009).
27. X. Yue, H. Chen, H. Qu, R. Min, G. Woyessa, O. Bang, and X. Hu, Sensors **20**, 6643 (2020).
28. T. Erdogan, J. Lightwave Technol. **15**, 1277 (1997).
29. F. Hindle, E. Fertein, C. Przygodzki, F. Durr, L. Paccou, R. Bocquet, P. Niay, H. G. Limberger, and M. Douay, IEEE Photonics Technol. Lett. **16**, 1861 (2004).
30. X. Hu, D. Kinet, P. Mégret, and C. Caucheteur, Opt. Lett. **41**, 2930 (2016).
31. G. Khanarian, Opt. Eng. **40**, 1024 (2001).
32. J. Yu, X. Tao, and H. Tam, Opt. Mater. **28**, 181 (2006).